2990 *Macromolecules* **2010**, *43*, 2990–3003
DOI: 10.1021/ma901842q

Macromolecules
ARTICLE

Formation and Collapse of Single-Monomer-Thick Monolayers of Poly(*n*-butyl acrylate) at the Air−Water Interface

Kevin N. Witte,[†] Sumit Kewalramani,[‡] Ivan Kuzmenko,[§] Wei Sun,[†] Masafumi Fukuto,[‡] and You-Yeon Won*,[†]

[†]*School of Chemical Engineering, Purdue University, West Lafayette, Indiana 47907,* [‡]*Condensed Matter Physics and Materials Science Department, Brookhaven National Laboratory, Upton, New York 11973, and* [§]*X-ray Science Division, Advanced Photon Source, Argonne National Laboratory, Argonne, Illinois 60439*

Received August 18, 2009; Revised Manuscript Received January 12, 2010

ABSTRACT: The behavior of poly(*n*-butyl acrylate) (PnBA) spread at the air−water interface has been studied for a full range of surface coverages and several molecular weights. At low and intermediate surface coverages, the surface pressure−area isotherm behavior of the polymer is found to follow the expected scaling laws. In the dilute regime the pressure is an increasing function of surface coverage and a decreasing function of molecular weight. In the semidilute regime the surface pressure becomes independent of molecular weight, and a Flory exponent for the two-dimensional radius of gyration is found to be $\nu = 0.57 \pm 0.02$. Beginning in the high coverage concentrated regime, at a surface pressure of around 15 mN/m, and through the full coverage regime (where the water in the subphase is fully covered and not exposed to air), X-ray reflectivity (XR) measurements show the formation of a continuous water-free monolayer (i.e., one monomer thick) film of the polymer. At surface concentrations above the transition point to the full coverage regime (alternatively called the "collapsed" regime hereafter for the reason that will become apparent below), Brewster angle microscopy (BAM) shows that the excess polymer material does not distribute uniformly in the polymer film layer but instead leads to formation of micrometer-scale isolated globular domains of roughly uniform size. Further, it was observed that the number of such domains increases as the surface polymer concentration is increased, whereas the size of the globular domains is largely unaffected by the concentration variation. X-ray grazing incidence diffraction (GID) indicates that these domains are regions of bulklike (amorphous) polymer. These and other observations, including the invariant nature of the monolayer throughout the compression (confirmed by XR), the plateau nature of surface pressure−area isotherm throughout the collapsed regime, and the reversible nature of the domain formation (evidenced by BAM), suggest that the globular domains formed at high surface concentrations of PnBA are in a type of coexistence with the uniform monolayer. A simple thermodynamic model considering the entropic penalty of confining the polymer chains to monolayer, the translational entropy of the domains, and the surface energy of the interface is made in order to understand the behavior of the polymer as it becomes excluded from the monolayer. This argument suggests that the excess polymer should form a single large domain in order to minimize the large surface energy at the water−polymer interface. The presence of many small domains suggests the domains are kinetically trapped in a local, rather than global, equilibrium.

1. Introduction

The spreading of insoluble or amphiphilic molecules on a liquid substrate, especially water, at the interface of another fluid, such as air or oil, has a long and illustrious history. The first published observations of this kind are due to Benjamin Franklin, who in 1774 reported the results of his famous experiment in which he placed a teaspoon of oil on the surface of Clapham Pond and noted that the surface ripples of the water became strongly suppressed.[1] Since then, a wide range of materials, ranging from surfactants[2,3] to proteins[4−6] to synthetic polymers,[7−9] have been spread at fluid−fluid interfaces. The study of such systems has added to our knowledge about such diverse topics as the functioning of our lungs[6] to the behavior of polyelectrolyte polymer brushes.[10,11]

The careful study of synthetic polymers at the air/water interface began with Crisp,[7,12] who measured surface pressure (Π) versus area per monomer isotherms for a wide variety of polymeric materials that contained amphiphilic character within the chain, e.g., ester or ether linkages. Classifying the polymers into four categories based upon molecular architecture, he found that each group had a general characteristic isotherm. The first group contains soft amorphous polymers, such as poly(vinyl acetate) and polyacrylates, which spread readily to give stable films and "gelate", meaning they become elastic with respect to shear stress, at high surface pressures (20−30 mN/m). The second group contains "tough" amorphous polymers, such as polymethacrylates, which give stable films and "gelate" at intermediate pressures (0−10 mN/m). The third and fourth groups are composed of semicrystalline polymers and form films that are unstable or collapse at low surface pressures (0−5 mN/m), respectively.[7]

With the advent of the scaling laws of polymer physics,[13] reliable quantitative analysis and deeper physical understanding of the surface pressure−area isotherms for synthetic polymers became possible. These two-dimensional (2D) systems typically exist in four regimes.

The first is a dilute or virial regime, where for low surface coverages (Γ) or, inversely, high areas per chain (A) the surface pressure can be written, in analogy with bulk osmotic pressure, as a virial expansion of the ideal mixture[9,14]

$$\Pi = \frac{RT\Gamma}{M_n}(1 + A_2\Gamma + ...) \quad (1)$$

Here R is the gas constant, T is temperature, M_n is the polymer number-average molecular weight, A_2 is the second virial coefficient, and Γ is the surface coverage in mass per area. In the past

*To whom correspondence should be addressed. E-mail: yywon@ecn.purdue.edu.

 Published on Web 02/25/2010

this equation was used to determine the second virial coefficient,[15] which determines if the net two-body interactions between monomers are repulsive ($A_2 > 0$), causing the chains to swell relative to a purely random coil configuration, or are attractive ($A_2 < 0$), causing the chains to contract relative to the random coil. In three dimensions the swelling and contracting of the chains is mediated by the solvent leading to the concept of "solvent quality". A swollen chain is said to "like" the solvent more than itself and is thus in a "good" solvent. Similarly, a contracted coil is said to "dislike" the solvent and is thus in a "poor" solvent. When these two tendencies are balanced and the coil is in a purely random (governed by Gaussian statistics) configuration, the polymer is said to be in a "theta" solvent. This solvent quality concept provides a useful framework for discussing the configurations of polymers confined to 2D geometries. If the coils are swollen (Gaussian), then the interface is said to be a good (theta) solvent even though there is no "true" solvent present. Although due to difficulties in measuring such low pressures the above equation is now not frequently used for the determination of the solvent quality that an interface presents to an adsorbed polymer,[9] the equation provides us with one useful insight, namely that for low surface coverage the surface pressure is inversely proportional to the molecular weight.

In the semidilute regime the individual polymer coils begin to have numerous strong interactions with the other coils on the surface. Here the scaling theories of de Gennes,[14] as extended to the 2D case,[8] state that the surface pressure can be expressed in terms of an ideal solution of so-called "correlation blobs".[16] This idea results in a power law, independent of molecular weight, relating the surface pressure to the surface coverage

$$\Pi \sim \Gamma^{y} \tag{2}$$

where the exponent y is related to the Flory exponent, ν, for the radius of gyration by

$$y = \frac{2\nu}{2\nu - 1} \tag{3}$$

When the interface acts as a good solvent, mean field theory[16] predicts a Flory exponent of $\nu = 3/4$, which has been confirmed experimentally.[8,15,17−20] In the theta condition, $\nu \approx 1/2$ is expected, and computer simulations have found $\nu = 0.505$.[21] However, experimentally determined values have typically been found greater than $\nu \approx 0.52$[9] and have varied greatly even between the same authors using the same materials.[8,15] The difficulty is mainly due to the narrow region of surface coverage in which the semidilute regime exists.

The third regime is the concentrated regime. In analogy with three-dimensional polymer solutions, here the polymer chains are strongly interacting, but these interactions are strongly self-screened. Thus, the polymers adopt random Gaussian coil configurations.[16]

In the final high surface coverage regime the polymer film begins to collapse. The surface pressure at which the collapse begins is characteristic of the polymer being studied but can be correlated to the stiffness of the chain.[7] Previously, we demonstrated for monolayers of poly(*n*-butyl acrylate) at the air-water interface that this point is where the monolayer completely covers the surface in a uniform phase, and the critical pressure can be calculated from the surface tensions of the two layered interfaces as

$$\Pi_0 = \gamma_{\text{air-water}} - (\gamma_{\text{air-polymer}} + \gamma_{\text{polymer-water}}) \tag{4}$$

where $\gamma_{\text{A-B}}$ is the surface tension between phases A and B.[11,22] Crisp originally proposed that the collapse must be due to monomers leaving the interface based upon changes in the apparent surface dipole moment, which is due to the orientation of the molecular dipoles of the chains' polar groups at the interface, with surface coverage through the collapse regime.[7] Using electron microscopy of high surface coverage poly(vinyl acetate) films, Ries and Walker observed "large bulbous masses" on the film surfaces and hypothesized that monomers that have left the surface are forming a multilayer structure.[23] However, neutron reflectivity experiments of poly(methyl methacrylate) showed large quantities of water entrained in the film which would indicate the potential existence of looped structures, i.e., sections of the polymer chains that are not adsorbed onto the surface but are still anchored to the interface by at least one monomer on each end.[24,25] Gavranovic et al. also observed such "bulbous masses" with a length scale on the order of 10 μm using Brewster angle microscopy (BAM) of poly(*tert*-butyl methacrylate).[26] Hysteresis experiments showed that these structures, once formed at high surface compression, persisted to lower surface pressures, upon expansion of the monolayer, with a simultaneous decrease in the associated plateau of the isotherm. These observations were attributed to possible entanglements within the bulklike domains of this glassy polymer.

Mann et al. have observed films of polydimethylsiloxane (PDMS) at the air−water interface using BAM. PDMS belongs to Crisp's second group of "tough" amorphous polymers as its films "gelate" at a surface pressure of about 8.9 mN/m.[27] These authors showed that at very low surface pressures (~0 mN/m) the PDMS films form distinct domains of high and low surface coverage; these are reminiscent of those formed by low molecular weight lipid molecules.[28] These domains are believed to cause the observed deviations from ideal mixture behavior in the dilute regime for the PDMS system. At surface pressures above the collapse transition regions thickness greater than a monolayer were observed. These domains were observed to coalesce over time.

In this work we report a study of the surface structures and properties of poly(*n*-butyl acrylate), which is a soft amorphous polymer, $T_g = -55$ °C,[29] and belongs in Crisp's first group, through all four surface coverage regimes. This is the first such study of a soft polymer in the near theta condition (as will be discussed below) for such a wide range of surface coverages. At low to intermediate surface polymer concentrations, measurements of the surface pressure vs area isotherms for a variety of molecular weights showed excellent agreement with the simple virial expansion and power law scaling theories presented above. Within the full surface coverage (i.e., "collapsed") regime, X-ray reflectivity (XR) showed the formation of a complete water-free polymer monolayer of monomer thickness, while BAM imaging again shows the presence of micrometer-scale globular domains of regular size in the polymer layer. X-ray grazing incidence diffraction (GID) indicates that no molecular crystallization is involved in the formation of these structures. These and other results suggest that in the collapsed regime the PnBA monolayer undergoes a transition upon compression from the monolayer state to the globular structure. A simple free energy analysis was performed by considering that each chain that becomes excluded from the surface during compression can form either a small single chain globule or a large aggregate with other chains. Consideration of the free energy due to interfacial tension effects as well as mixing entropy of the two structures, and the entropic penalty of confining the polymers suggests that the system should equilibrate as a single macroscopically large domain of bulk polymer due to the high interfacial energy of the system. However, we find that the domains appear to be kinetically trapped in a more localized equilibrium.

2. Experimental Section

Materials. Copper(I) bromide (CuBr) was purchased from Sigma-Aldrich. Before use, it was washed with glacial acetic acid, ethanol, and finally anhydrous ethyl ether. The clean salt was then dried under vacuum for 4 h at 50 °C. The dried product

Table 1. Names, Number-Average Degrees of Polymerization (DP_n) and Molecular Weights (M_n), and Polydispersity Indices (PDI) of the Poly(*n*-butyl acrylate) (PnBA) Polymers Used in This Study

sample name	DP_n	M_n (g/mol)[a]	PDI
$PnBA_{45}$	45	5935	1.14
$PnBA_{76}$	76	9908	1.10
$PnBA_{111}$	111	14 394	1.12
$PnBA_{168}$	168	21 700	1.11
$PnBA_{269}$	269	34 645	1.58

[a] Each chain contains an ATRP initiator fragment which increases the molecular weight above $DP_n \times M_{nBA}$.

was stored in a nitrogen atmosphere until use. *n*-Butyl acrylate (nBA) monomers were purchased from Fluka and passed through an inhibitor (hydroquinone monomethyl ether) removal column purchased from Scientific Polymer Products, Inc., immediately before use. The purified monomer was bubble degassed with argon for 30 min and kept under an argon atmosphere until use. Anhydrous *N,N*-dimethylformamide (DMF) was purchased from Aldrich and stored over molecular sieves of pore size 4 Å in an argon atmosphere prior to use. *N,N,N′,N′,N″*-Pentamethyldiethylenetriamine (PMDETA) and methyl 2-bromopropionate were purchased from Sigma-Aldrich and used as received. Silica flash gel was purchased from Silicycle and used as received. All other solvents were purchased from Mallinckrodt Chemicals and used as received.

PnBA Synthesis. The polymer was synthesized via atom transfer radical polymerization (ATRP) as reported previously.[11] First, the CuBr catalyst was sealed into a round-bottom flask under an inert atmosphere. The nBA monomers and DMF cosolvent were then added to the flask, while maintaining the inert atmosphere, such that the desired degree of polymerization can be achieved and the DMF constitutes 10% of the total initial volume (slightly higher volumes were used for the two highest molecular weight polymers). The PMDETA ligand is added to dissolve the catalyst. The flask was then placed in an oil bath at 90 °C and stirred for 10 min. Methyl 2-bromopropionate was then added to initiate the polymerization reaction. The final ratio of initiator to catalyst to ligand was 1:1:1. The reaction was then allowed to proceed for 30−60 min (depending upon the desired molecular weight) which was sufficient for near complete conversion. The flask was then removed from the oil bath and the contents diluted with dichloromethane. This solution was then passed through a silica gel column. The resulting clear solution is vacuum distilled to remove excess solvent and dried under vacuum at 120 °C for 6 h.

Characterization. The number-average degree of polymerization was calculated from the ^{1}H NMR spectrum taken on a Bruker ARX300 spectrometer operated at 300 MHz. Deuterated chloroform ($CDCl_3$) containing 0.10% v/v tetramethylsilane as the internal reference was used as the solvent. The polydispersity index (PDI) was determined by gel permeation chromatography (GPC) using a Waters Breeze HPLC machine containing two Phenogel columns with pore sizes 0.05 and 0.4 mm. The eluent was tetrahydrofuran (THF) at a flow rate of 1 mL/min at 30 °C. Polystyrene standards with molecular weights ranging from 2290 to 357 400 g/mol were used to correlate elution time to molecular weight. Table 1 summarizes the molecular characteristics of the polymers used in this study.

Contact Angle Measurements. The contact angles of water on PnBA and water on oxidized silicon (as a model hydrophilic substrate for comparison) in air were measured using a Ramé-Hart Automated model 500 goniometer. Data were collected and analyzed using DROPimage Advanced software. PnBA homopolymer was spin-coated onto a 2 cm × 2 cm silicon wafer (Silicon Inc., (100) surface) from a 10 wt % solution in chloroform. A single drop of water was placed on the clean, dry surface and allowed to evaporate. Starting at time zero and then every 5 min the contact angle was measured five times on each side of the drop. The average value along with the drop width and height were recorded. Sample data from one representative trial are presented in Figure S5 of the Supporting Information. The contact angle at time zero is defined as the static contact angle and is found to be 84.2 ± 3.8°. The Young equation can then be used to calculate the surface tension of water on a PnBA film.

Isotherm Measurements. Surface pressure−area isotherms were collected using a KSV 5000 Langmuir trough (15.0 cm × 51.0 cm × 1.0 cm) within a plexiglass chamber. The hydrophobic trough and hydrophilic symmetric moving barriers were cleaned by repeated rinsing with ethanol followed by deionized water. The surface pressure was measured by the Wilhelmy method using a platinum plate, located equidistant from each barrier, which was cleaned by rinsing with ethanol and water and then flamed. Deionized Millipore water (18 MΩ·cm resistivity) was used as the substrate, the surface of which was cleaned via aspiration prior to spreading. The cleanliness of the surface and probe was checked by compressing the water surface at 3 mm/min and monitoring the surface pressure. If total change in the pressure was greater than 0.2 mN/m, the surface and probe were recleaned and measurement retaken until the surface pressure change was below this threshold. A 1.0 mg/mL solution of PnBA polymer in chloroform was prepared fresh for each trial and spread dropwise on the water surface using a Hamilton microsyringe. The surface pressure was monitored after deposition until it reaches a plateau value, typically 3−4 h. The isotherm was then recorded while compressing the barriers at 3 mm/min.

Hysteresis Isotherms. The hysteresis surface pressure−area isotherms were collected using a KSV minitrough (maximum area: 75 mm × 302 mm) with a filter paper Wilhelmy probe at 23 °C. The surface and monolayer were prepared as above. The first compression−expansion cycle was recorded at about 4 h after spreading the monolayer on pure water, and a barrier speed of 3 mm/min was utilized. The second and third compressions were performed respectively at about 7 and 22 h after the film was spread. A barrier speed of 12 mm/min was used for these compressions. A two-cycle hysteresis measurement with the cycles done at barrier speeds of 2 and 4 mm/min showed no difference in the observed trend. Varying the barrier speed between 2 and 12 mm/min did not show any effect on the measured isotherms for either trough.

Macroscopic Drop. The KSV 5000 trough was prepared as above, including checking for surface cleanliness by compressing the water surface without polymer present. A vial containing the pure, dry polymer, and a clean glass Pasteur pipet were placed on a balance, and the mass was recorded. Recording of the surface pressure as a function of time at a fixed area, A = 765 cm^2, was begun to obtain a baseline value. After 35 min polymer was removed from the vial using the pipet tip. A pendent drop of the polymer was allowed to form on the tip and carefully placed on the water surface while recording the surface pressure. After the polymer had detached from the tip and settled on the surface the mass of vial with the remaining polymer and the pipet was again recorded. The difference was found to be 2.0 mg, which corresponds to a surface concentration of Γ = 26.1 mg/m^2. This is about 17 times larger than the concentration at the highest compression. The system was monitored for a further 2.5 h until a plateau, indicating equilibrium, was observed.

Brewster Angle Microscopy (BAM). Simultaneous BAM and isotherm measurements were carried out by using an optical setup based on the design by Honig and Mobius[30,31] and a KSV Minitrough (7.5 cm × 30.0 cm × 0.5 cm, 23 °C). The samples were prepared as described above, and the surface pressure was monitored by the Wilhelmy method using a filter-paper plate. A laser beam (argon ion laser, λ = 488 nm, 100 mW fiber-optic output) that was p-polarized via a Glan-Taylor calcite polarizer was incident on the solution surface (spot diameter ∼1 mm) at 53.3° from the surface normal, the Brewster condition for the bare water surface. The nonzero reflected intensity caused by the presence of the polymer film was used to image the film-coated

interface. The reflected beam was passed through an achromatic lens (f = 30 mm), and the image was captured by a CCD camera at a magnification of 20.2 and a resolution of the order of 10 μm in the focused region.

X-ray Measurements. X-ray reflectivity (XR) and grazing incidence diffraction (GID) measurements were carried out at Beamline 9-ID C of the Advanced Photon Source (APS) at Argonne National Laboratory (Argonne, IL), using the liquid surface spectrometer operated at an X-ray wavelength of λ = 1.284 Å. The polymer film was prepared as described above on an R&K trough (Riegler & Kirstein GmbH; 12.1 cm × 24.0 cm × 0.5 cm, 23 °C), which was enclosed in a sealed aluminum box filled with humidified helium in order to reduce background scattering. Consider a situation in which the incident X-ray beam makes an angle α to the surface ($x-y$ plane) and the scattered X-ray beam makes an angle β to the surface and an azimuthal angle ψ to the plane of incidence. In typical XR measurements,[32] the specularly reflected intensity I at $\beta = \alpha$ and $\psi = 0$ is measured as a function of the incident angle α or the wave vector transfer $q_z = (4\pi/\lambda)\sin(\alpha)$ along the surface normal (z-axis). XR data were collected using a NaI scintillation detector with angular acceptances of $\Delta\beta = 0.15°$ and $\Delta\psi = 0.15°$. The reported signal is the difference between the intensity measured at the specular position ($\psi = 0$) and the background intensity measured at ψ offsets of ±0.15°. The background-subtracted intensity was normalized to the incident beam to obtain the reflectivity $R(q_z) = I(q_z)/I_0$. For GID,[32] the incident angle was fixed at $\alpha = 0.10°$, which was below the critical angle for total reflection ($\alpha_c = 0.128°$ for the water/vapor interface at λ = 1.284 Å). With an incident beam size of 0.10 mm (v) × 0.5 mm (h), the X-ray illuminated footprint had an area of 57 mm × 0.5 mm. GID data were collected using a set of Soller slits (angular acceptance: $\Delta\psi = 0.16°$) and a linear position-sensitive Mythen detector (0.05 mm/channel or $\Delta\beta = 0.005°$/channel). In terms of the wave vector transfer **q**, the corresponding resolutions were $\Delta q_{xy} \approx (2\pi/\lambda)\Delta\psi = 0.014$ Å^{-1} and $\Delta q_z \approx (2\pi/\lambda)\Delta\beta = 0.0004$ Å^{-1}.

The fitting of the XR data was carried out by using the standard "box" model for the average electron density profile $\langle\rho(z)\rangle$,[32] which is based on the combination of error functions. In the present analysis, the monolayer between the subphase ($\langle\rho\rangle = \rho_{water} = 0.333$ electrons/Å^3) and the vapor above ($\langle\rho\rangle = 0$) was represented by a box of height ρ_1 and thickness l_1, and the two interfaces were smeared out by a common Gaussian roughness σ. The reflectivity corresponding to this box-model profile $\langle\rho(z)\rangle$ was calculated by the matrix method of the Parratt formalism[33,34] for $q_z < 0.1$ Å^{-1} and using the kinematic (Born) approximation[32] for $q_z \geq 0.1$ Å^{-1}. The theoretical reflectivity curve thus calculated was fitted to the data for $q_z \geq 0.05$ Å^{-1} by varying the box-model parameters (ρ_1, l_1, σ) and allowing a small variation (less than 5%) in the overall multiplicative factor to take into account a possible error in the incident-beam normalization. It should be noted that XR is sensitive only to the profile $\langle\rho(z)\rangle$ itself, i.e., not to exactly how $\langle\rho(z)\rangle$ is constructed. The box parameters were strongly coupled such that different sets of these parameters could produce a nearly identical density profile. However, the best-fit profiles themselves were found to be well-defined. In particular, the maximum density $\rho_{max} = \max(\langle\rho(z)\rangle)$ and the distance L between the two z positions at which the derivative $d\langle\rho(z)\rangle/dz$ were at local maxima could be determined with relatively small uncertainties. These profile-derived quantities, ρ_{max} and L, are plotted in Figure 9.

3. Analysis and Discussion of Experimental Results

The surface pressure−area isotherms were measured for the five different number-average degrees of polymerization (DP_n) summarized in Table 1. In Figure 1 these results are plotted as surface pressure, Π, versus surface mass concentration, Γ. Each curve represents an average of several raw curves about the

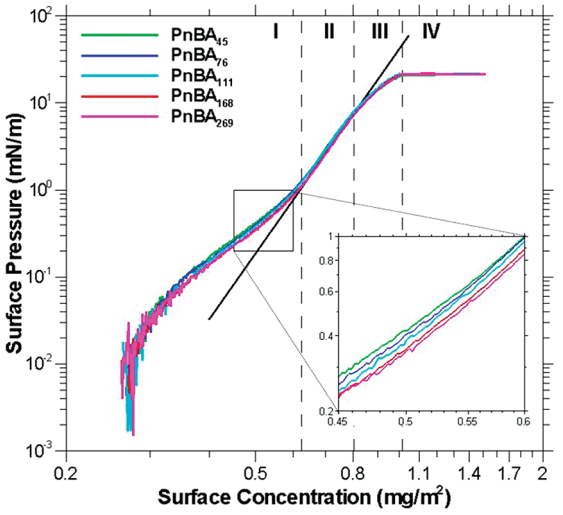

Figure 1. Surface pressure (Π) versus surface concentration (Γ) for PnBA with chain molecular weights of M_n = 6K, 10K, 14K, 22K, and 35K. The dilute (I), semidilute (II), concentrated (III), and collapsed (IV) regimes are separated by the three vertical dashed lines. The semidilute regime is fit to the scaling theory power law, indicated by the straight line in the log−log plot, and shows $\nu \approx 0.57$ (see eqs 2 and 3). The inset shows details of the virial/dilute regime in the region indicated by the box in the main figure and contains data from the surface coverage range of 0.45−0.60 mg/m^2 and surface pressure range of 0.2−1.0 mN/m.

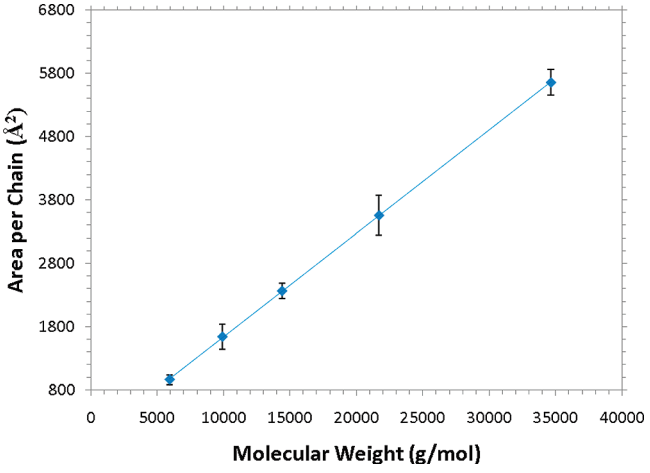

Figure 2. Area per chain of the transition point as a function of molecular weight (M_n). Error bars represent a 90% confidence interval on the mean for each molecular weight.

plateau transition point value of the surface coverage. A total of 2−8 runs, each beginning at the same surface concentration, were used in the averaging process for each molecular weight depending upon their initial level of agreement. For a given molecular weight, the transition point was found by locating the largest change in slope along the isotherm. The surface concentrations at these points are averaged, and all the curves shifted on the linear ordinate by addition of a constant such that all the transition points equaled the average (to take into account the uncertainties associated with the polymer concentration measurements and also the possible accidental loss of polymer to the subphase or to the trough surfaces during the spreading process). At this point, all the concentration values overlapped within a certain range, and any nonoverlapping data points were discarded (the low and high surface coverage extremes). The surface pressure at each remaining point was averaged and shifted up slightly (on the linear abscissa) such that the minimum value of the surface

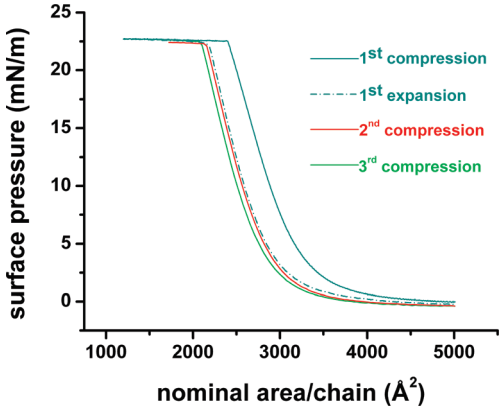

Figure 3. Hysteresis surface pressure (Π) versus nominal area per chain (α) isotherms for $PnBA_{111}$ showing the first compression−expansion cycle and two subsequent compressions. It is evident from the figure that the differences between the second and the third isothermal compression curves are much smaller than those between the first and the second compressions due to the lesser extent of compression applied in the second compression course than in the first.

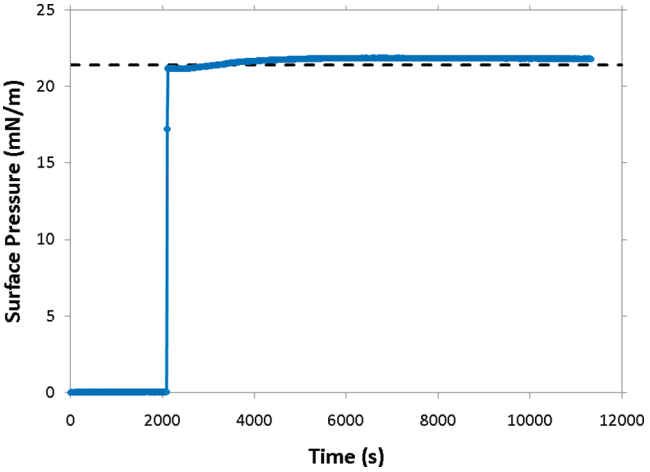

Figure 4. Surface pressure (Π) versus time (t) for a single macroscopic (2 mg) drop of pure $PnBA_{111}$ placed on a clean water surface at t = 2085 s. The dashed line indicates the transition point surface pressure determined from the Π−Γ isotherms (Figure 1). The dots represent the actual data points taken at 15 s intervals and demonstrate how rapidly the pressure jump occurs.

pressure is zero (this shift is typically < 0.02 mN/m); this vertical shift is to take into account the uncertainty in the surface pressure measurement and zero calibration. The resultant Π−Γ isotherms are presented in the log−log presentation in Figure 1. The effect of the averaging process on the raw data is illustrated in Figure S1 of the Supporting Information where all the raw curves are plotted with the final curve.

As highlighted in the figure, there exist four surface coverage regimes of distinct surface pressure behavior. The viral regime occurs at low surface coverages up to ~0.65 mg/m^2. The data here exemplifies why it is difficult to use eq 1 to determine the solvent quality presented by the interface. The scatter in the data (exaggerated by the log−log presentation) makes fitting of the virial expansion impossible. However, by examining the plot near the transition to the semidilute regime, as shown in the inset, it can be seen that the inverse dependence of the surface pressure on molecular weight (predicted in the virial expansion equation) does hold for the PnBA polymers employed here. In particular, the inset to Figure 1 clearly demonstrates the inverse relationship between the surface pressure and polymer molecular weight in this regime. The $PnBA_{45}$ seems to deviate slightly from this trend at the higher surface coverages shown in the inset, but these discrepancies are probably due to the near oligomeric nature of such a short chain and its propensity to adsorb to the surfaces of the trough and barriers. We do not, however, find the pressure to decrease as M_n^{-1} (as suggested by eq 1). Instead, we find a much slower decay with the exponent being approximately −1/10; see Figure S2 of the Supporting Information. This is probably due to observing the pressure too close to the semidilute regime and also the noise in the measurements at very dilute surface concentrations and not to large micrometer-scale domains as observed with PDMS at the air−water interface by Mann et al.[27] Such domains, as shown later in Figures 5 and 6, were not observed in this dilute regime of the PnBA system. The presence of the regions of differing density in the PDMS films causes the characteristic sharp transition to the semidilute regime at a very low surface pressure. We note that such a transition is similar to that observed with micrometer-sized silica particles at the air−water interface[35] and differs from the (ideal-gas-like) gradual change in surface pressure observed here for PnBA films in the dilute concentration regime.

The semidilute regime begins at $c^* \approx 0.64$ mg/m^2 and ends at $c^{**} \approx 0.76$ mg/m^2; these points are marked in Figure 1 by two vertical lines. Here we see that, as predicted, the isotherms collapse onto a single curve independent of molecular weight. As illustrated in the figure, eqs 2 and 3 can be employed to fit a power law to the surface pressure data in this regime. From such a fit an estimate of the 2D Flory exponent can be made. In this case the data for the $PnBA_{269}$ polymer was utilized to find value of the exponent of $\nu = 0.57 \pm 0.02$, which is in agreement with other published values[8,9,15,26] for polymers in a poor solvent condition at the air−water interface. Using this value of the Flory exponent and the definition of the overlap concentration,[8] $c^* \sim N^{1-2\nu}$ where N is the chain length, we expect that c^* should vary with molecular weight to the −0.14 power. However, we did not find any significant variation of c^* with molecular weight although this is most likely due to limits in the data resolution and the estimating procedure. As expected,[16] we also did not find any variation of c^{**} with molecular weight, but the same caveats regarding data resolution and the estimating procedure still hold. See Figure S3 of the Supporting Information for plots of c^* and c^{**} versus molecular weight. One final note concerning the semidilute regime: While it may appear that c^{**} has been set too low, when compared with c^*, this is in fact an artifact of the log−log presentation. Both c^* and c^{**} were defined to be the surface concentrations where the actual data deviated by ~5% positively and negatively, respectively, from the best fit power law.

The concentrated regime begins at c^{**} and shows a marked departure from the best fit power law of the semidilute regime. Throughout this regime, presumably, the random polymer coils are slowly compressed, resulting in a pure polymer monolayer as will be demonstrated below. This process continues until the projected area of the monomer hard core volumes is reached and 2D compression cannot continue. At this stage the final collapsed regime is reached.

The collapsed regime can be seen at the highest surface coverages of Figure 1. The observed plateau remains even up to surface coverages of 4.6 mg/m^2 with no further upturn in the pressure as has been observed for similar polymers, such as glassy poly(*tert*-butyl methacrylate).[26] Such a plateau is usually indicative of some type of phase change occurring in the monolayer. The collapsed regime begins with the sudden change of slope that occurs at 1.01 ± 0.01 mg/m^2. We term this point of each isotherm the "transition point" and demonstrate in Figure 2 that it occurs at the same surface coverage value for each molecular weight. In the figure, the transition point is plotted in units of Å^2/chain as a

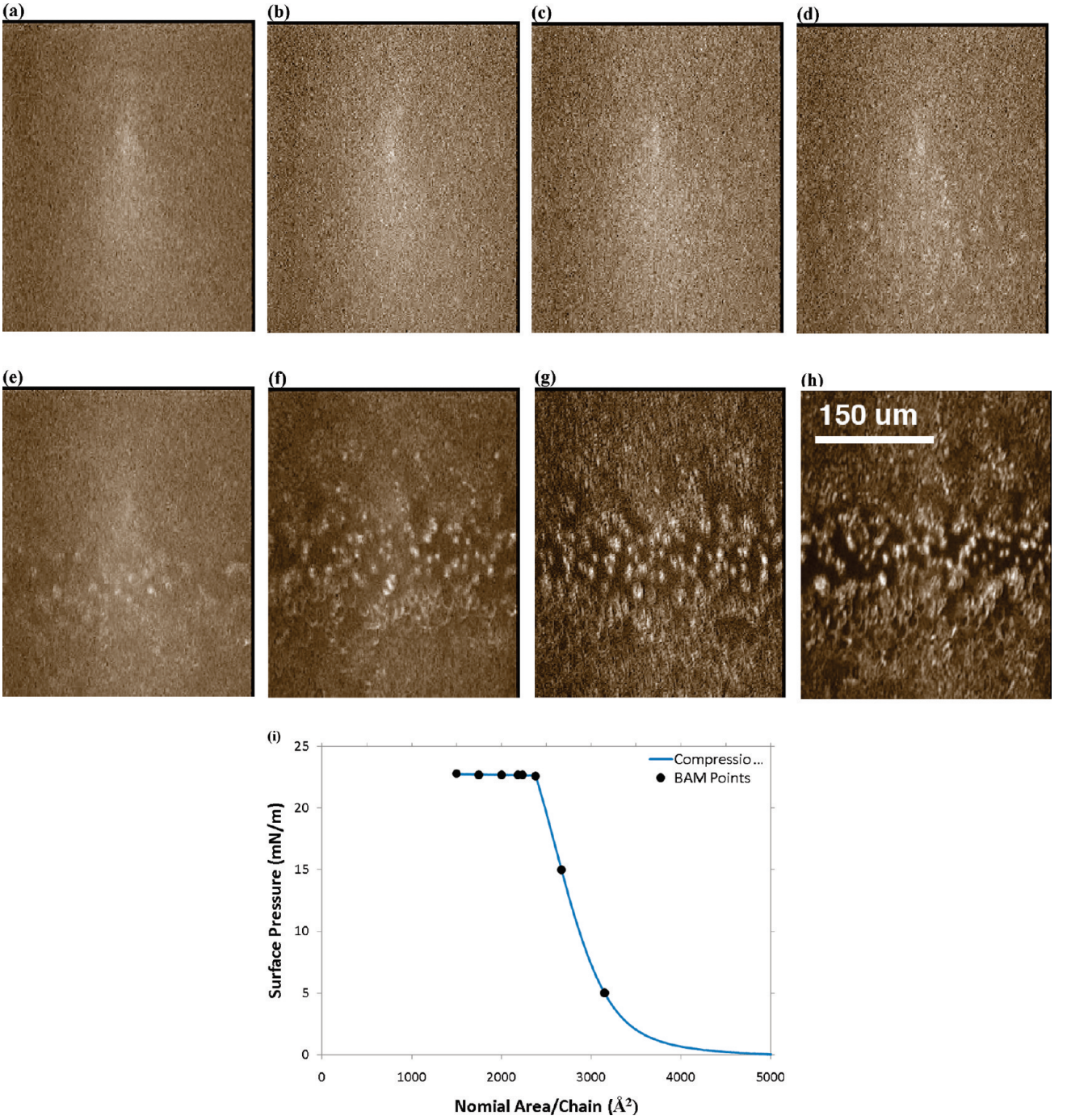

Figure 5. Brewster angle microscopy (BAM) images (317 μm × 398 μm) of a $PnBA_{111}$ film during compression for α = 3149 (a), 2667 (b), 2379 (c), 2235 (d), 2185 (e), 2003 (f), 1748 (g), and 1500 Å^2/chain (h). The compression isotherm shows the surface pressures relating to the above areas per chain where the images were taken (i).

function of the molecular weight in g/mol. Linear regression gives a line with slope 0.163 ± 0.002 (Å^2 mol/g) and a statistically insignificant y-intercept. This yields two results. First, it is obvious that the value of the transition point, when plotted in molecular weight independent units such as Å^2/monomer or mg/m^2, is also independent of molecular weight. Second, the limiting value of 20.9 ± 0.3 Å^2 is obtained, by evaluating the regressed line at the molecular weight on a single monomer, for the area of an n-butyl acrylate monomer. This value agrees with our previous result obtained with a different analysis.[11] Since the behavior of the polymer at high surface concentrations is independent of molecular weight, we choose (arbitrarily) to use the $PnBA_{111}$ polymer as a case study of the collapsed state.

Hysteresis experiments were performed to assess the reversibility of the isotherms and structures contained therein. The results for the $PnBA_{111}$ at 22 °C are shown in Figure 3 for one complete compression and expansion cycle, and two subsequent compressions and are plotted in terms of surface pressure (Π) versus the nominal area per chain (α); here we use the term "nominal" because α is calculated by dividing the area of the air−water interface (A_0) by the total number of polymer chains spread at the air−water interface (n_T), regardless of whether or not the polymers form flat homogeneous layers. The first compression shows a transition point identical to that found above. The pressure at this point was about 1.6 mN/m higher than the values shown in Figure 1; this difference is likely due to

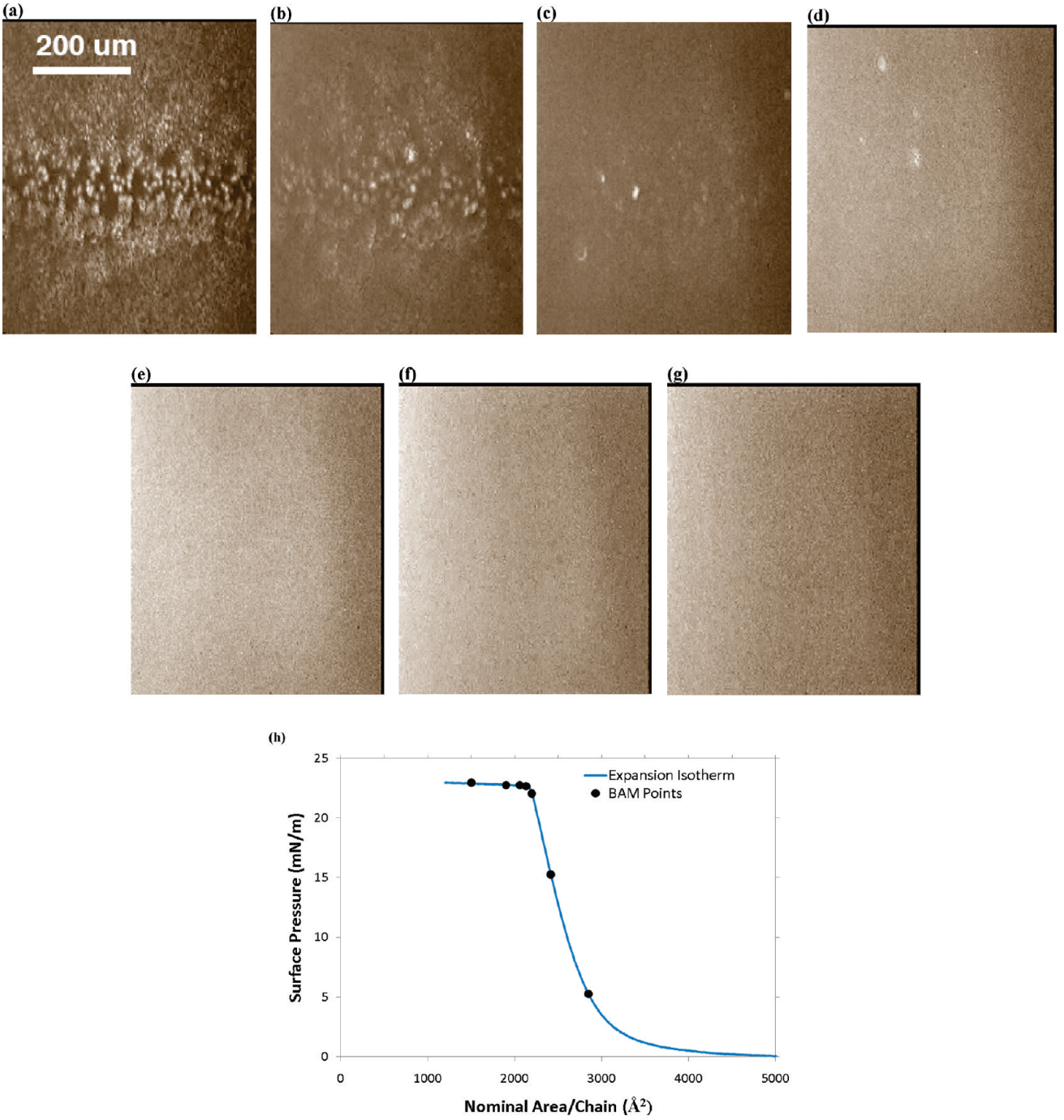

Figure 6. Brewster angle microscopy (BAM) images (519 μm × 651 μm) of a $PnBA_{111}$ film during expansion for α = 1503 (a), 1900 (b), 2058 (c), 2130 (d), 2197 (e), 2413 (f), and 2845 Å^2/chain (g). The expansion isotherm shows the surface pressures relating to the above areas per chain where the images were taken (h).

small errors in calibration of the balances and is nonetheless within an acceptable range (especially given other differences in experimental details, for instance, the differences in Wilhelmy plates (platinum versus filter paper) and temperature (22 °C versus 25 °C)). The most obvious effect is that the curve shifts to the left with each subsequent step. This indicates there is less material than expected on the (compressible) surface. In addition, subsequent compressions nearly overlap previous expansions. This shift of the isotherm is not due to the slow relaxation of the compressed structure (caused for instance by entanglements of the chains). The possibility of such behavior can be ruled by placing a single macroscopic drop of the pure polymer on a clean water surface. If significant entanglement effects are present, we would expect the polymer to spread somewhat slowly with a finite slope to the surface pressure as the transition pressure is reached due to slow disentanglement dynamics. Instead, Figure 4 shows that the spreading of $PnBA_{111}$ is instantaneous and complete (the drop was deposited onto the water surface at t = 2085 s on the scale of the ordinate in Figure 4). The full-coverage transition pressure, indicated by the dashed line, is reached immediately through a step change in surface pressure. Thus, an entangled three-dimensional melt can instantaneously form a monolayer that completely covers the surface at the greatest level of surface coverage possible. The shape of the curve following the initial pressure jump (i.e., the very slight increase in surface pressure that occurred for the next few thousand seconds) is presumably due to

the observed slower spreading of the remaining bulk polymer across the monolayer covered surface to form more spread multilayer structures with thicknesses greater than a monolayer. The original macroscopic globule of bulk polymer remained visible to the naked eye on the surface for roughly 5 min after being placed on the water surface. On the microscopic length scales, however, the final structure of the polymer film is not expected to be laterally uniform for the reason that will be discussed below.

Taken together, this implies a loss of material from the measurable surface in some fashion as the film is compressed through the isotherm plateau. This could be losses to the subphase (though unlikely because of the strong hydrophobic nature of the polymer side chains), losses under the barriers, or losses due to adsorption on the walls of the trough or barriers. More importantly, the expansion isotherms show the same general qualitative shape as those measured during compression. There does, however, seem to be a slight rounding of the curve at the transition point upon expansion. This lack of qualitative hysteresis indicates relatively quick relaxation dynamics, as expected from the low glass transition of PnBA ($T_g \approx -55$ °C[29]), and a likely lack of entanglements in collapsed monolayer.

Brewster angle microscopy (BAM) was utilized to visualize the surface of the monolayer throughout the compression and expansion isotherms. Figure 5 shows selected BAM images taken during the compression isotherm. The surface is uniform for high area/chain greater than the transition value, however, at and below this value small micrometer-sized domains appear and become more numerous and brighter with continued compression; note that the precise size of the domains could not be determined because of the limited resolution of the BAM images ($\approx$10 μm). Figure 6 shows selected BAM images taken during the expansion isotherm. In this instance, the domains become less numerous with expansion along the plateau before disappearing altogether at the transition point. These domains might be the same types of "bulbous masses" observed by Ries and Walker in their electron microscopy studies.[23] In view of their reversibility the structures are probably best understood in terms of Crisp's theory that monomers are squeezed out of the interface at high compression.[7] This would necessarily lead to coexistence of molten bulklike domains with the monolayer intervening. X-ray grazing incidence diffraction (GID) measurements of films above the transition point, i.e., at 1295 Å^2/chain, showed no evidence for crystalline structures in the layer (see Figure S4 in the Supporting Information). Thus, the domains observed by BAM must be amorphous and not due to the spatial rearrangement of the monomers into regular structures.

Figure 7a plots the number density of domains ($= N_D/A_0$ where N_D is the number of domains in the system) against the nominal area per chain (α). The experimental number densities were determined from the BAM images of Figures 5 and 6 by counting the number of bright domains inside a long narrow box of known area along the center of the images. The nominal area per chain values for the expansion isotherm have been shifted up (by adding a constant value) in Figure 7 to account of the hysteresis effect described previously. The relative errors for each data point are expected to be large since only one image was available at each area/chain and only a small portion of the image is clear enough to distinguish individual domains. Given this limitation, though, a clear, monotonically decreasing trend in the data is established, and both the compression and expansion data agree quite well. Further, there was no observed coalescence of the domains which were stationary relative to each other, moving only in the direction of surface compression; short video clips demonstrating this behavior are available in the Supporting Information. Using the domain number density data, the number-average radius of the domains (R) can also be calculated for each given value of α using the equation $R = [3(n_T - A_0/\alpha_0)/(2\pi N_D \rho)]^{1/3}$, where α_0 denotes the area-per-chain quantity at the transition point and ρ is the melt density of the polymer in units of number per volume. The results of these calculations are presented in Figure 7b. As shown in the figure, the domain radius is found to be of the order of a few hundred nanometers and largely invariant throughout the collapsed regime ($\alpha < \alpha_0$). By taking the value of R at $\alpha = 1500$ Å^2/chain (i.e., $R = 410$ nm), it is estimated that each domain contains $\sim 6.53 \times 10^6$ PnBA chains.

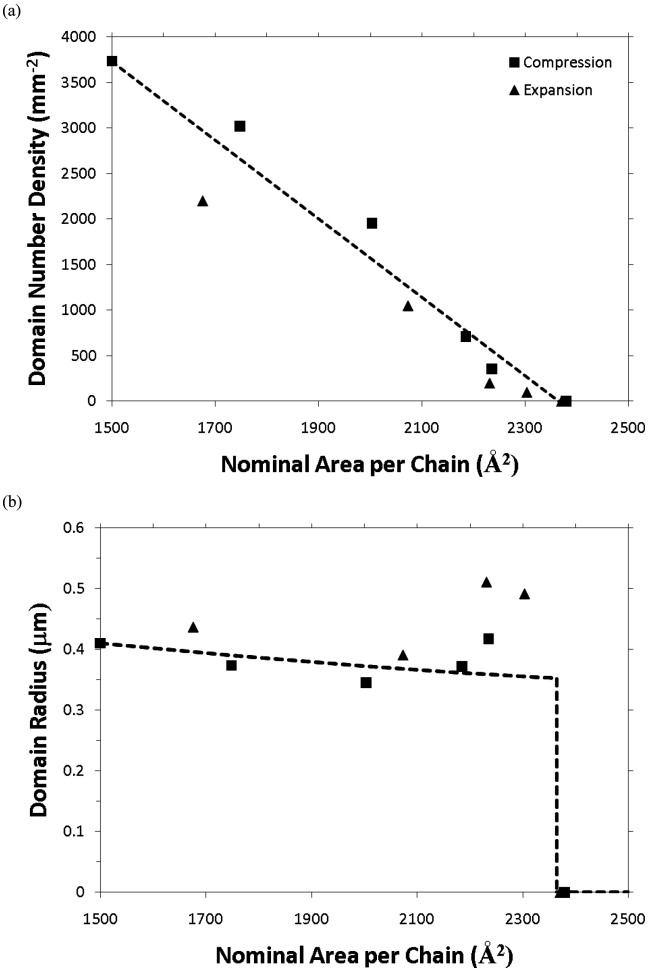

Figure 7. (a) Plot of domain number density versus the nominal area per chain (α). The squares and triangles are data determined from the BAM images of a compression (Figure 5) and expansion (Figure 6) isotherm, respectively. (b) Plot of domain radius versus the nominal area per chain. The domain radius values have been estimated from the data in (a). The broken lines are guides to the eye.

Table 2. Points Where the X-ray Reflectivity Measurements on the $PnBA_{111}$ Film Were Taken, Including Method of Controlling the Surface (Constant Pressure or Area), and the Value or Range of the Surface Pressure (Π) and Area per Chain (α)

position no.	method	pressure (mN/m)	α (Å^2/chain)
1	constant area	1−1.5	3974
2	constant pressure	~7.6	3207−3133
3	constant pressure	~15.0	2779−2729
4	constant pressure	~20.0	2536−2513
5	constant area	21.54−21.64	1779
6	constant area	~21.7	1295

The monolayer nature of the PnBA film at the air−water interface was verified by X-ray reflectivity (XR). The measurements were taken at various points along the surface pressure−area isotherm while holding the film at either a constant area or surface pressure. The type of measurement taken at each point is summarized in Table 2. The measured reflectivity,

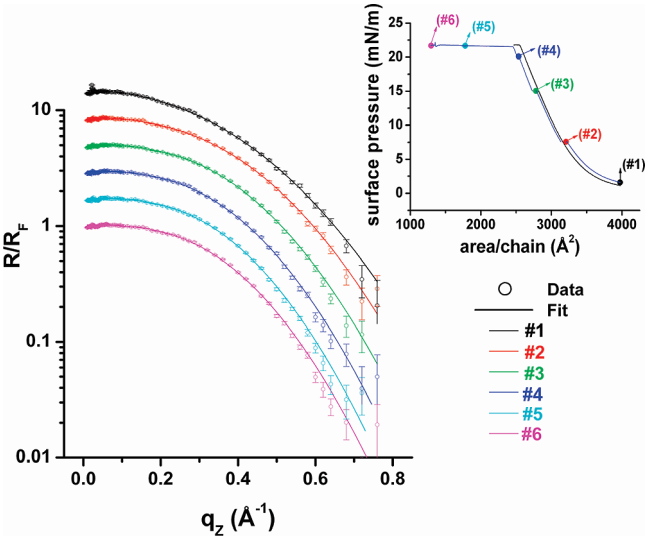

Figure 8. Measured X-ray reflectivity (XR) data (discrete symbols) for the $PnBA_{111}$ monolayer. The measured reflectivity, $R(q_z)$, is normalized by the Fresnel reflectivity, $R_F(q_z)$, of an ideally flat and sharp water−vapor interface. The individual data sets have been independently shifted vertically for clarity of the presentation. The inset shows the surface pressure−area isotherm of the same system and indicates the area/pressure conditions at which the XR data were taken. The solid lines in the reflectivity plot represent the best model fits to the experimental data.

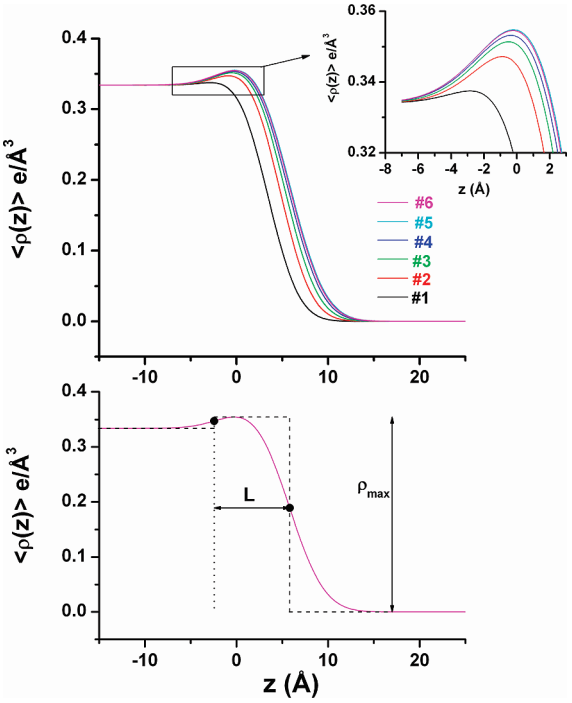

Figure 9. (top) Average electron density profiles estimated for the $PnBA_{111}$ monolayer at the air−water interface at various surface area/pressure conditions. These density profiles represent the best fits to the respective XR data presented in Figure 7 (we used the identical set of color notations). The inset clearly demonstrates that the electron density of the monolayer is an increasing function of the surface concentration of the polymer. (bottom) Sample plot illustrating how the monolayer thickness (L) and density (ρ_{max}) values have been calculated from a best-fit electron density profile. The two black dots indicate the positions of local extrema in the gradient of the density profile, and L is defined as the distance between the two extrema.

normalized by the Fresnel values, is displayed as symbols in Figure 8. The solid curves in Figure 8 are the best fits to the experimental data, and the corresponding average electron density profiles are shown in Figure 9. The details of the fitting can be found in the Experimental Section. For all probed values of the area per chain, the derived electron density profiles are consistent with the presence of a single (i.e., continuous) high-density layer at the interface. Moreover, compression past 15 mN/m, i.e., into the concentrated regime, results in little further change in the density profile, even at points along the plateau of the isotherm. This indicates that XR is not sensitive to the small domains that were observed by BAM and that the surrounding polymer film remains in the same monolayer state along the isotherm plateau. The XR's lack of sensitivity to the small globular domains (observed by BAM) suggests that these regions have a three-dimensional structure different from that of the surrounding monolayer. This conclusion is arrived at by considering the three factors that determine the intensity of the reflection: electron density contrast across the interface, interfacial roughness, and interfacial curvature. Because a good signal is detected from the monolayer, it can be assumed that the density contrast is sufficient and that the roughness is not extreme. Since there is no reason to expect these parameters will be different in the domain regions, surface curvature remains as the only explanation for the lack of sensitivity. We believe from the XR and BAM data that the domain surfaces have excess curvature relative to the flat monolayer region which greatly reduces the measured intensity. For instance, the reflectivity from a convex-downward globular domain should be much smaller than that from a flat surface because the radiation incident on the curved surface would have, on the downstream side, incident angles that are larger than the nominal incident angle, which leads to significantly reduced reflectivity ($R < R_F \sim q_z^{-4}$). Also, the upstream part of the surface of the globular domain will be shaded and will therefore give a negligible contribution to the measured reflectivity.

It should be noted that the negligible to zero reflectivity from the domains may negatively contribute to the overall reflectivity of the sample. If, for example, the domains covered 40% by area of the surface, one could expect the measured intensity to be only 60% of that at the transition point where collapse begins (i.e., at the complete coverage with no domains). However, no significant change in the measured reflectivity signal is observed along the isotherm plateau, which suggests that the area fraction of the domains is quite low. In fact, we estimate, from the data shown in Figure 7, the projected surface coverage of the domains to be ~2.0% by area, for example, at a compression condition of $\alpha = 1500$ Å^2/chain. Thus, the surface regions covered by the small domains would not contribute significantly to the measured reflectivity. One might question then whether or not the same sensitivity limitation should apply to the GID measurements. It should be noted that unlike XR, the GID signal does not originate solely from the interface, but rather GID probes the existence and extent of an in-plane crystal structure near the interface. It is estimated that at the surface coverage examined ($\alpha = 1295$ Å^2/chain) approximately half of the polymer molecules exist in the monolayer phase and the rest of the molecules in the globular domains. Therefore, it is reasonable to expect a strong GID signal from the sample if there existed any crystalline phases; monolayers of long-chain alcohols, for instance, have been shown to exhibit strong GID peaks.[36] Conversely, the absence of any crystalline diffraction clearly confirms the amorphous nature of the PnBA film throughout the sample, and the sensitivity argument used in the interpretation of the XR data is irrelevant to the conclusion from the BAM measurements. Further, it should be pointed out that the ATRP-synthesized PnBA polymers are expected to be non-crystalline because of their atactic configuration in stereochemical structure.

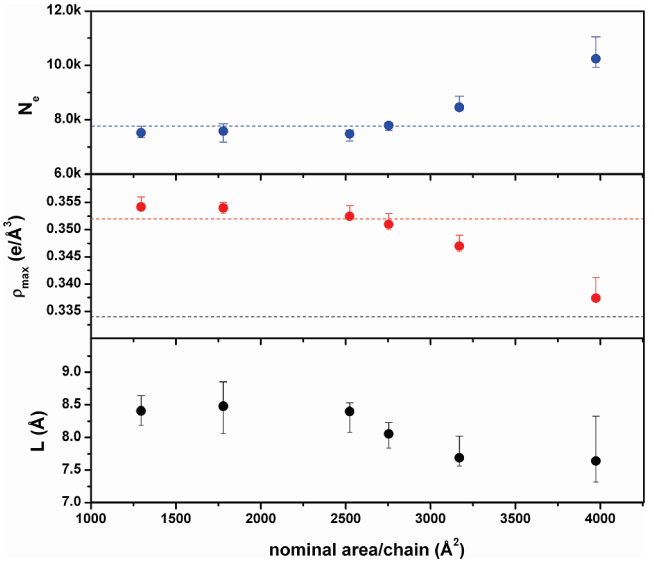

Figure 10. Dependences of the thickness (L), electron density (ρ_{max}), and number of electrons per chain (N_e) properties of the $PnBA_{111}$ monolayer at the air−water interface on the nominal area per chain condition. The results were extracted from the best-fit electron density profiles as described in the main text. The black dotted line denotes the value of ρ_{max} for bulk water (= 0.334 $e^-/Å^3$) at 23 °C. The red dotted line represents the electron density of PnBA in the bulk state (ρ_{max} = 0.352 $e^-/Å^3$). In the collapsed regime, the number of electrons associated with the monolayer, N_e, is defined as $\rho_{max}L\alpha_0$ where α_0 denotes the area per chain at the full-coverage transition (or collapse transition) point (here we used a value of $\alpha_0 \approx 2500$ $Å^2$/chain); that is, for the points along the isotherm plateau, the area per chain value for the monolayer structure is taken to be constant at 2500 $Å^2$/chain, which is the value of α at the onset of the surface pressure plateau (see the main text for explanation). In the partial surface-coverage regime (i.e., at $\alpha > \alpha_0$), the same quantity is estimated using $\rho_{max}L\alpha$. The blue dotted line represents the value of N_e estimated for the monolayer structure (= 7770 e^-/chain) on the basis of the monomer chemical structure and molecular weight of $PnBA_{111}$.

Figure 10 plots the area-per-chain dependence of three monolayer-associated parameters, derived from the best-fit density profiles. The layer thickness L is defined as the distance between the two maximum-slope positions in the density profile (as illustrated in Figure 9). The maximum value ρ_{max} in the electron density profile can be taken as a measure of the electron density within the monolayer. The number of electrons (per chain) associated with the monolayer N_e can be calculated, in the collapsed regime, as the product $\rho_{max}L\alpha_0$ where α_0 denotes the area per chain at the full-coverage transition (or collapse transition) point (here we used a value of $\alpha_0 \approx 2500$ $Å^2$/chain, which was the value determined from the isotherm); the use of α_0 (instead of the nominal area per chain, α) in the above equation is that the globular domains formed at $\alpha < \alpha_0$ do not give rise to a measurable reflectivity (as explained earlier). In the partial surface-coverage regime (i.e., at $\alpha > \alpha_0$), N_e is estimated using the equation $\rho_{max}L\alpha$. The monolayer has a higher electron density than water (black dotted line). In this regime the electron density of the monolayer (ρ_{max}) is seen to increase monotonically with surface pressure; only after the surface pressure plateaus, ρ_{max} also becomes independent of α. In addition, the measured thickness of the layer also increases with surface pressure, when $\alpha > \alpha_0$. Further, it can be seen that the number of electrons per chain in the film decreases with increasing surface pressure until the pressure reaches ~15 mN/m, the concentrated regime. All three parameters remain constant along the isotherm plateau. In particular, the profile-derived number of electrons per chain matches very nearly the predicted number of 7770 electrons/chain for monodisperse $PnBA_{111}$ (denoted by a blue dotted line in the figure). Along the isotherm plateau, the electron density of the monolayer agrees well with the value for the bulk polymer (red dotted line). These observations lead to the conclusion that the polymer film is truly a *monolayer*, i.e., only one layer of the polymer with monomer thickness, and that by and beyond the onset of the plateau this monolayer is essentially free of water. This differs from the findings of Henderson et al., who found that poly(methyl methacrylate) films contained large amounts of entrained water molecules.[25]

We would like to point out that even when the globular domains are present under high compression, the polymer film exists predominantly in the form of a monolayer; that is, the number density of the globular domains is generally significantly low. For instance, as shown in Figure 7a, even at the lowest surface area probed (i.e., at α = 1500 $Å^2$/chain), the domain density is measured by BAM to be only about 3.75×10^{-3} per μm^2. If the PnBA film is examined at this surface area condition by AFM (e.g., after Langmuir−Blodgett (LB) deposition onto a solid support), the globular structure will be detected, on average, only in 1 out of 67 2 μm × 2 μm area scan images. Therefore, it should be noted that the observation of the globular domains in the present study is not in contradiction to the AFM data reported in our previous publication[11] in which the LB-deposited PnBA film has been shown to be atomically flat (see Figure 1d of ref 11). Also, we note that the prediction of the significantly low projected-area fraction of the globular domains (relative to the monolayer area) is also consistent with the XR result that the reflectivity profile is insensitive to further compression once the full surface coverage point is reached.

4. Discussion on the Globular Domains

Taken all together, our experimental results indicate that in the collapsed regime (i.e., once the water surface is fully covered with PnBA) further lateral compression causes surplus polymer molecules to form discrete globular domains of regular size and amorphous nature that are in coexistence with the original monolayer structure. We expect that any polymer excluded from the monolayer will accumulate on water−polymer interface as opposed to the air−polymer interface because $\gamma_{water-polymer} < \gamma_{air-polymer}$, which means the latter interface has a higher energy of formation. Specifically, at room temperature $\gamma_{air-polymer}$ = 33 mN/m for PnBA[37] and $\gamma_{water-polymer}$ = 19.6 mN/m for PnBA[11] where we have determined the latter quantity by contact angle measurements (see Figure S5 of the Supporting Information).

For the purpose of this analysis it is important to know what configuration an individual chain, which has been excluded from the monolayer, would initially adopt. One possibility is a flat "pancake-like" configuration where the chain forms a two-dimensional coil at the surface. In this scenario the chain pays an entropic penalty for confining its contour to two dimensions. This penalty can be estimated using the methods of Doi and Edwards[38] for a polymer constrained, in this case perpendicular to the surface, in a potential well, in units of k_BT, as

$$f_{confine} = \frac{\pi^2 N b^2}{6d^2} \quad (5)$$

Here, b is the monomer size (i.e., the statistical segment length) and N is the renormalized number of monomers. For the $PnBA_{111}$ sample these values are 12.32 Å and 27.75, respectively, assuming a characteristic ratio of $C_\infty \approx 7$ for the polymer. The thickness of the coil perpendicular to the surface, d, is determined from the polymer density, ρ, and the area per chain at the transition point, α_0, and is found to be $1/\alpha_0\rho$ = 9.36 Å. This yields a confinement penalty of 79 k_BT. In addition, the exclusion of the chain creates additional interfacial area associated with the thickness of the coil, d. Assuming the chain assumes a two-dimensional

random coil conformation, the work to create the additional surface area can be estimated as

$$f_{\text{interface}} = 2nld\gamma_{\text{water-polymer}} \quad (6)$$

where n is the number of C−C bonds along the backbone of the chain (= 2 × 111 in the $PnBA_{111}$ case) and l is the C−C bond length (= 1.54 Å). This gives an interfacial penalty of 305 k_BT. The area parallel to the surface does not contribute as an area equal to that created by the coil is covered up on the monolayer surface. Similar calculations, assuming the formation of a compact disk-shaped structure of thickness d, give $f_{\text{confine}} \approx 97\ k_BT$ and $f_{\text{interface}} \approx 182\ k_BT$.

The other possible configuration the chain could take is a three-dimensional globule, which we assume for simplicity is a half-sphere. The volume of this hemisphere is $1/\rho = 2.21 \times 10^4$ Å^3. The entropic penalty of confining a single chain in this volume can be estimated as $3f_{\text{confine}}$ from eq 5, where d is now the dimension of confining well which was estimated from a cube of the same volume as the hemisphere. The entropic penalty was found to be 26 k_BT. The energetic cost of forming the new interfacial area is calculated from

$$f_{\text{interface}} = (2\pi r^2 - \pi r^2)\gamma_{\text{water-polymer}} \quad (7)$$

where r is the radius of the hemisphere, giving an interfacial penalty of 72 k_BT. Clearly, the 3D globule is the energetically more favorable configuration.

A similar argument can be made to confirm that the PnBA polymer forms a two-dimensional monolayer on the water surface. Consider a polymer that is at the transition point where the water surface is barely fully covered with the polymers; it thus occupies α_0 units of area per chain in the monolayer. If the chain forms a globule of hemisphere shape as above, the system will have a polymer−water interfacial area of $2\pi r^2$, a polymer−air area of πr^2, and an air−water area of $\alpha_0 - \pi r^2$, all on a per-chain basis, and the same confinement penalty as the globule case above. Accounting for the three interfacial energies ($\gamma_{\text{air-water}} = 73$ mN/m), the combined free energy of this configuration would be 442 k_BT. In contrast, if the polymer forms the flat 2D monolayer, the system only has polymer−air and polymer−water interfaces of area α_0 on a per-chain basis, but also has the 2D confinement penalty described above. This state's free energy is 381 k_BT, thus showing that the flat 2D-confined monolayer configuration is favored whenever the air−water interfacial area can be covered with polymer. In a related note, eq 4 should almost certainly contain corrections related to the confinement entropy penalty. However, since $\Pi \sim -\partial F/\partial A$ and the gradient of the confinement free energy is expected to be small near the transition point, any correction to eq 4 will be negligible.

The reversible nature of the formation of the globular microdomains (as confirmed by BAM), and the variation of the relative populations (as evidenced by BAM), along with the invariance of the quantitative characteristics of both the globular domains and the surrounding monolayer structure with respect to compression (as evidenced by XR) suggest the picture that these two states might be in thermodynamic equilibrium. Further, the transition from the monolayer state to the globular state, induced by surface pressure, might be a thermodynamic phase transition (likely of the first order because it occurs at a constant surface pressure). The preceding argument on the globular configuration of a single chain excluded from the interface provides a framework with which to further develop a theoretical understanding of the observations from a thermodynamics point of view.

Consider a macroscopic air−water interfacial area A_0 on which n_T chains are spread. The chains have a characteristic bulk 3D density ρ and 2D close-packed area per chain α_0. The chains are spread such that $A_0/n_T < \alpha_0$, and n_0 (= $n_T - A_0/\alpha_0$) chains are excluded from the surface. These excluded chains form the aforementioned globules which begin to locally aggregate. Once large enough, the aggregated globules become bulklike domains which incorporate the chains of the underlying monolayer into themselves. At some level of aggregation the domains reach an equilibrium with the remaining single chain globules. For simplicity, we will consider a monodisperse ensemble of domains in thermodynamic coexistence with the globules. The domains are assumed to be spherical caps characterized by an aspect ratio $\beta = H/2R$, where H is the height of the cap and R is the radius at the air interface (see Scheme 1). The total system free energy thus has contributions not only from the creation of interfacial area and the entropy of chain confinement but also from the translational entropy of the domains and globules across the surface. We choose the free energy reference state to be the condition where the n_0 excluded chains are all in the isolated globule state with no large domains formed.

Scheme 1. Cartoon Illustrating the Assumed Configuration of the PnBA Monolayer at the Air−Water Interface at Surface Concentrations above the Transition Point in the Collapsed Regime[a]

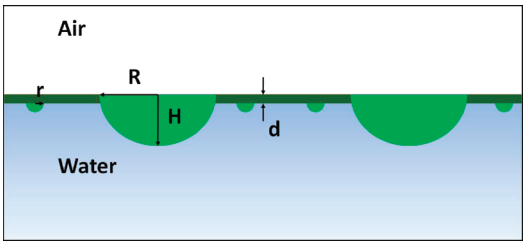

[a] The dark green regions are those containing polymer chains that are adsorbed to the water surface. This monolayer region is characterized by a thickness d. The light green regions contain polymer chains not adsorbed to the interface. The large domains contain polymers in a bulklike state and are characterized by a radius R and height H. The small regions are single condensed chain globules characterized by a radius r.

The interfacial free energy is calculated from the change in interfacial area from the reference state to the final state multiplied by the polymer−water surface tension, from here on out abbreviated γ_{PW}. The surface area of the final state can be calculated from the original flat area A_0 and the domain and globule geometries as

$$A_{\text{final}} = A_0 + N_D SA_D + n_1 2\pi r^2 - N_D \pi R^2 - n_1 \pi r^2 \quad (8)$$

Here we have added the surface area per spherical cap SA_D, which can be determined as a function of the domain radius and aspect ratio from

$$SA_D = \pi R^2 + 4\pi R^2 \beta^2 \quad (9)$$

and also added the area per single chain globules which have radius r and are assumed to be hemispherical. The flat monolayer area covered by the domains and globules is subtracted off in the last two terms of eq 8. The area per domain and the area per globule are multiplied by the number of each feature, N_D and n_1, respectively. The reference surface area is calculated in a similar fashion except there are only n_0 globules of radius r and no large domains

$$A_{\text{ref}} = A_0 + n_0 2\pi r^2 - n_0 \pi r^2 \quad (10)$$

Thus, the interfacial free energy contribution to the total system free energy, in units of k_BT, is

$$F_{\text{interface}} = \gamma_{PW}(4N_D \pi R^2 \beta^2 + \pi r^2 (n_1 - n_0)) \quad (11)$$

The free energy due to the translational entropy of the globules and domains across the surface can be calculated utilizing the Sackur−Tetrode equation for an ideal gas modified to two dimensions. This equation requires that each domain or globule

is volume-less and does not interact with any other, which is a reasonable assumption in our case, because both the domains and unimeric globules are dilutely dispersed across the surface. In two dimensions the Sackur−Tetrode equation says the absolute entropy of species i, S_i, can be written

$$\frac{S_i}{k_B} = n_i\left(\ln\left[\frac{2\pi m_i k_B T}{h^2 n_i} A_0\right] + 2\right) \tag{12}$$

where n_i and m_i are the number and mass per particle of species i and h is Planck's constant. Assuming each domain contains n_D chains, the mass of a domain can be determined to be $m_D = m_1 n_D$, where m_1 is the mass of a single chain and $n_D = \rho V_D$. The volume, V_D, of a domain is again determined from the radius and aspect ratio

$$V_D = \pi\beta R^3 + \frac{4}{3}\pi\beta^3 R^3 \tag{13}$$

Thus, the total translational free energy for the system (including the reference state), in units of $k_B T$, is

$$F_{trans} = n_0\left(\ln\left[\frac{2\pi m_1 k_B T}{h^2 n_0} A_0\right] + 2\right) - N_D\left(\ln\left[\frac{2\pi m_1 k_B T}{h^2 N_D}\rho V_D A_0\right] + 2\right) - n_1\left(\ln\left[\frac{2\pi m_1 k_B T}{h^2 n_1} A_0\right] + 2\right) \tag{14}$$

Again, the Doi−Edwards formalism[38] can be used to calculate the free energy of a polymer chain confined in a potential well. When the dimensions of the well are much larger than the end-to-end distance $b\sqrt{N}$, then the energy per chain is related to the well volume

$$\frac{F_{confine}}{k_B T} = -\ln(l_x l_y l_z) \qquad l_x, l_y, l_z \gg b\sqrt{N} \tag{15}$$

where l_i is a well length in a single coordinate direction. If one of the lengths is less than $b\sqrt{N}$, then that coordinate's contribution becomes

$$\frac{F_{confine}}{k_B T} = -\ln\left[\frac{8d}{\pi^2}\exp\left(-\frac{\pi^2 N b^2}{6d^2}\right)\right] \qquad d < b\sqrt{N} \tag{16}$$

In each case these terms require a reference state to maintain dimensionality. We arbitrarily choose a bulk state with a volume that exactly cancels the nonexponential terms that arise in eqs 15 and 16. The final simplified confinement free energy, in units of $k_B T$, is

$$F_{confine} = n_1\frac{\pi^2 N b^2}{2r^2} - n_0\frac{\pi^2 N b^2}{2r^2} - \frac{N_D \pi R^2}{\alpha_0}\frac{\pi^2 N b^2}{6d^2} \tag{17}$$

The first term in eq 17 is the confinement free energy penalty of chains in the final state that remain in the unimeric globule configuration. The second term is the confinement term associated with the reference state. The final term is the decrease in free energy due to releasing the chains at the interface, in the area in contact with the large domains, from the confining monolayer.

Finally, the system is subject to a mass conservation constraint. The total number of chains in the system, n_T, a fixed known quantity, is equal to the number of chains in the monolayer, A_0/α_0, plus the sum of the number of chains in the domain, $N_D n_D$, and the number of remaining single chain globules, less those chains incorporated from the monolayer into the domains, $N_D \pi R^2/\alpha_0$.

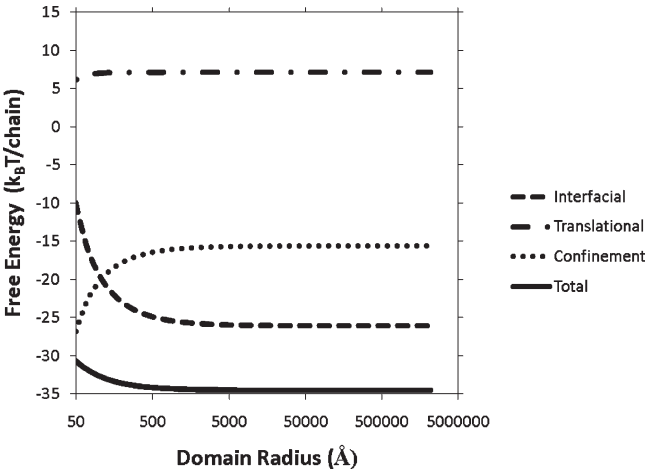

Figure 11. Results of thermodynamic analysis of the coexistence of bulk domains with highly compressed monolayer. Calculations were performed for the $PnBA_{111}$ polymer where renormalized $N = 27.75$, $\rho_0 = 4.518 \times 10^{-5}$ Å^{-3}, $\alpha_0 = 2364$ Å^2/chain, and $b = 12.32$ Å. Plot of the total system free energy along with the interfacial, translational, and confinement contributions to the total energy as functions of the domain radius R.

$$n_T = N_D n_D + n_1 + \frac{A_0 - N_D \pi R^2}{\alpha_0} \tag{18}$$

Rearranging, this relation allows for the determination of the number of domains, N_D, as a function of the domain size and shape

$$N_D = \frac{\alpha_0 n_T - \alpha_0 x n_0 - A_0}{\alpha_o \rho V_D - \pi R^2} \tag{19}$$

Here we have written the number of single chain globules, n_1, as a fraction, x, of the total number of chains excluded from the interface, n_0. Thus, the total system free energy, in units of $k_B T$, is

$$F_{total} = F_{interface} + F_{trans} + F_{confine} \tag{20}$$

which is a function of the domain radius, R, the domain aspect ratio, β, and the fraction of chains remaining as single-chain globules, x. This simple model is fairly limited, particularly due to its restrictions on the size and shape of the domains, but we believe it gives a reasonable qualitative picture of system behavior.

Figure 11 shows a representative calculation of the components on the right-hand side of eq 20 (scaled by n_T) as a function of domain radius R at A_0/n_T ($= \alpha$) $= 1500$ Å^2/chain (compare with Figure 5h) for fixed $\beta = 0.5$ (half-sphere) and $x = 0.01$. Note that the low end of range of radii is outside the range of validity for the calculation of the confinement energy; however, this range is pictured to clearly illustrate the trends. As expected, the interfacial energy is a decreasing function of domain radius. This means it favors larger domains in order to minimize the contact surface area between the polymer and the water. The translational and confinement terms oppose this tendency as shown in the figure since they are increasing functions of the radius. The translational entropy favors smaller domains because smaller domains means there are more of them. The confinement energy favoring small domains may seem counterintuitive because larger domains would relax the entropic confinement of the

chains. However, once the domains are large enough this entropic gain becomes negligible. Instead, by having more, smaller domains, a greater number of chains can be liberated from the confines of the monolayer; this effect thus favors smaller domains. Figure 11 also shows the resulting sum of these three contributions. Three important trends should be noted. First, the total free energy is negative, which implies that the formation of domains is favored over single chain globules. Second, the interfacial energy seems to dominate the system. Finally, the minimum of the free energy is found, asymptotically, when there is a single large domain. In this final equilibrium state we expect that there are no single chain globules left because these features not only suffer severe entropic losses associated with confinement but also greatly increase the interfacial area which has been shown to be highly unfavorable and in fact dominant over the translational and confinement entropy considerations. Thus, any small globules formed tend to aggregate with the domains, and once there, PnBA chains will not be able to escape from the domains as individual molecules due to both the large surface energy and confinement entropy penalties associated with such process. This is confirmed quantitatively in Figure S6 of the Supporting Information where we show that the minimum asymptotic free energy value occurs at $n_1 = 0$. Further, the effect of the domain aspect ratio is found to be negligible, as also demonstrated in Figure S6.

These results raise the obvious question as to why we do observe the formation of many micrometer-sized domains as opposed to a single large one. We feel the most reasonable answer is that the experimentally observed domains are not in true thermodynamic equilibrium but rather are kinetically trapped at a certain size. During compression a random subset of chains become excluded from the surface monolayer by steric effects. These chains form single chain globules which immediately begin to aggregate locally. However, at some point the domains become large enough that they can incorporate the underlying monolayer chains into a bulklike state. Once this happens, though, the domains become effectively tethered in place as translation would require rearranging the monolayer on a mesoscopic scale which would be very costly. Without the ability to translate across the surface and exchange material with other domains each domain becomes effectively isolated. Therefore, the system is not truly in global equilibrium, and the domains do not coalesce on a time scale observable in the BAM experiments. In fact, they appear to be in fixed locations relative to each other and only appear to move due to the compression; short movies are available in the Supporting Information. Rather, we suspect the domains are in some form of local equilibrium with the nearest chains in the monolayer as evidenced by the invariant nature of the monolayer throughout the compression (confirmed by XR), the plateau nature of surface pressure−area isotherm throughout the collapsed regime, and the reversible nature of the domain formation (evidenced by BAM).

5. Conclusions

Poly(*n*-butyl acrylate) has been studied over a wide range of surface concentrations covering the dilute/virial, semidilute, concentrated, and collapsed regimes. In the low surface coverage dilute regime the surface pressure was found to increase with a decrease in molecular weight as predicted by the classic virial expansion of the surface pressure in terms of a mass-based surface concentration. At the intermediate coverages of the semidilute regime, where the polymer coils first begin to strongly interact, the PnBA data were found to fit the molecular weight independent scaling theory for the surface pressure. The interface was found to be a slightly poor, near-theta condition solvent for PnBA. The 2D Flory exponent was found to be $\nu = 0.57 \pm 0.02$. In the high coverage collapsed regime BAM imaging indicates the presence of microscopic globular domains. On the basis of GID measurements, these regions are expected to be amorphous polymer that has become excluded from the interface. X-ray reflectivity, however, was not sensitive to the existence of these structures, instead showing a signature of a uniform monolayer at all surface pressures. In addition, the reflectivity demonstrated that the monolayer is nearly devoid of water molecules at pressures ≥15 mN/m, corresponding to the concentrated and collapsed regimes. A simple thermodynamic analysis on the polymers excluded from the monolayer above the transition point in the surface pressure−area isotherms was carried out by considering how the microscopic domains observed in the BAM images would affect the surface energy of the monolayer, the translational entropy of the chains, and the relative degree of confinement of the chains. This analysis suggests both the translational and confinement entropy contributions to the total system free energy favor the creation of many small domains. However, the surface energy term favors a single large domain of bulk polymer, and because this term dominates the other two, the excluded polymers are expected to be driven to form a large domain of bulk polymer as opposed to many smaller domains. The difference between this prediction and the observed phenomena is believed to arise because the domains, once they reach a certain size, become kinetically trapped and are no longer in true equilibrium.

Acknowledgment. The Purdue authors are grateful for financial support of this research from the National Science Foundation (DMR-0906567), the American Chemical Society Petroleum Research Fund (Grant 46593-G7), the 3M Company (Nontenured Faculty Award), and the Purdue Research Foundation Shreve Fund. The BNL contribution to this work was supported by the U.S. Department of Energy's Office of Basic Sciences (Division of Materials Science and Engineering) under Contract DE-AC02-98CH10886. Use of the X-ray facilities of the Advanced Photon Source (APS) at the Argonne National Laboratory was supported by the U.S. Department of Energy Office of Science, Office of Basic Energy Sciences, under Contract DEAC02-06CH11357. Special thanks are due to Professor Jeffrey Youngblood in the School of Materials Science and Engineering at Purdue University for generously allowing us to use their contact angle equipment.

Supporting Information Available: Demonstration of the averaging of the raw surface pressure-area isotherm data (Figure S1); power-law dependence of the PnBA surface pressure on the molecular weight of the polymer in the virial/dilute regime (Figure S2); dependences of the overlap concentration (c^*) and the semidilute-to-concentrated solution crossover concentration (c^{**}) of PnBA at the air-water interface on the molecular weight of the polymer (Figure S3); grazing incidence X-ray diffraction data from the PnBA111 monolayer at α = 1295 Å^2/chain (Figure S4); time-dependent contact angle, drop volume and contact area data obtained from evaporating water drops on bare silicon and spin-coated $PnBA_{111}$ surfaces (Figure S5); plot of the asymptotic system free energy value (F_{total}) when there is only one large domain ($R \rightarrow \infty$) as a function of the fraction, x, of chains remaining in the single chain globule state (Figure S6); two video clips demonstrating the static nature of the globular domains formed in the collapsed $PnBA_{111}$ monolayer at two different compression conditions, i.e., at α = 1500 and 2003 Å^2/chain (these movies can be viewed using VLC Player, which can be downloaded for free from the Internet). This material is available free of charge via the Internet at http://pubs.acs.org.

References and Notes

(1) Franklin, B.; Brownrigg, W.; Mr. Farish *Philos. Trans.* **1774**, *64*, 445–460.
(2) Prosser, A. J.; Franses, E. I. *Colloids Surf., A* **2001**, *178* (1−3), 1–40.
(3) Zana, R. *Adv. Colloid Interface Sci.* **2002**, *97* (1−3), 205–253.
(4) Taneva, S.; Keough, K. M. W. *Biophys. J.* **1994**, *66* (4), 1137–1148.
(5) Patino, J. M. R.; Sanchez, C. C. *Langmuir* **2004**, *20* (11), 4530–4539.
(6) Perez-Gil, J.; Keough, K. M. W. *Biochim. Biophys. Acta, Mol. Basis Dis.* **1998**, *1408* (2−3), 203–217.
(7) Crisp, D. J. *J. Colloid Sci.* **1946**, *1* (1), 49–70.
(8) Vilanove, R.; Rondelez, F. *Phys. Rev. Lett.* **1980**, *45* (18), 1502–1505.
(9) Esker, A. R.; Kim, C.; Yu, H. *Funct. Mater. Biomater.* **2007**, *209*, 59−110.
(10) Ahrens, H.; Forster, S.; Helm, C. A. *Phys. Rev. Lett.* **1998**, *81* (19), 4172–4175.
(11) Witte, K. N.; Hur, J.; Sun, W.; Kim, S.; Won, Y. Y. *Macromolecules* **2008**, *41* (23), 8960–8963.
(12) Crisp, D. J. *J. Colloid Sci.* **1946**, *1* (2), 161–184.
(13) de Gennes, P. G. *Scaling Concepts in Polymer Physics*; Cornell University Press: Ithaca, NY, 1988.
(14) Daoud, M.; Cotton, J. P.; Farnoux, B.; Jannink, G.; Sarma, G.; Benoit, H.; Duplessix, R.; Picot, C.; Gennes, P. G. D. *Macromolecules* **1975**, *8* (6), 804–818.
(15) Vilanove, R.; Poupinet, D.; Rondelez, F. *Macromolecules* **1988**, *21* (9), 2880–2887.
(16) Rubinstein, M.; Colby, R. H. *Polymer Physics*; Oxford University Press: New York, 2003; p 454.
(17) Takahashi, A.; Yoshida, A.; Kawaguchi, M. *Macromolecules* **1982**, *15* (4), 1196–1198.
(18) Kawaguchi, M.; Yoshida, A.; Takahashi, A. *Macromolecules* **1983**, *16* (6), 956–961.
(19) Kawaguchi, M.; Komatsu, S.; Matsuzumi, M.; Takahashi, A. *J. Colloid Interface Sci.* **1984**, *102* (2), 356–360.
(20) Kawaguchi, M.; Sauer, B. B.; Yu, H. *Macromolecules* **1989**, *22* (4), 1735–1743.
(21) Stephen, M. J.; McCauley, J. L. *Phys. Lett. A* **1973**, *A 44* (2), 89–90.
(22) Hur, J.; Witte, K. N.; Sun, W.; Won, Y.-Y. *Langmuir* **2010**, *26* (3), 2021–2034.
(23) Ries, H. E.; Walker, D. C. *J. Colloid Sci.* **1961**, *16* (4), 361–&.
(24) Henderson, J. A.; Richards, R. W.; Penfold, J.; Shackleton, C.; Thomas, R. K. *Polymer* **1991**, *32* (18), 3284–3294.
(25) Henderson, J. A.; Richards, R. W.; Penfold, J.; Thomas, R. K. *Macromolecules* **1993**, *26* (1), 65–75.
(26) Gavranovic, G. T.; Deutsch, J. M.; Fuller, G. G. *Macromolecules* **2005**, *38* (15), 6672–6679.
(27) Mann, E. K.; Henon, S.; Langevin, D.; Meunier, J. *J. Phys. II* **1992**, *2* (9), 1683–1704.
(28) Lee, K. Y. C. *Annu. Rev. Phys. Chem.* **2008**, *59*, 771–791.
(29) Roff, W. J. *Handbook of Common Polymers: Fibres, Films, Plastics, and Rubbers*; CRC Press: Cleveland, 1971.
(30) Honig, D.; Mobius, D. *J. Phys. Chem.* **1991**, *95*, 4590.
(31) Honig, D.; Mobius, D. *Thin Solid Films* **1992**, *210/211*, 64.
(32) Als-Nielsen, J.; McMorrow, D. *Elements of Modern X-ray Physics*; Wiley: Chichester, 2001.
(33) Lekner, J. *Theory of Reflection*; Dordrecht, Martin Nijhoff Publishers: Hingham, MA, 1987.
(34) Parratt, L. G. *Phys. Rev.* **1954**, *95* (2), 359–369.
(35) Hur, J.; Won, Y. Y. *Soft Matter* **2008**, *4* (6), 1261–1269.
(36) Berge, B.; Konovalov, O.; Lajzerowicz, J.; Renault, A.; Rieu, J. P.; Vallade, M.; Alsnielsen, J.; Grubel, G.; Legrand, J. F. *Phys. Rev. Lett.* **1994**, *73* (12), 1652–1655.
(37) Brandrup, J.; Immergut, E. H. *Polymer Handbook*, 3rd ed.; Wiley: New York, 1989.
(38) Doi, M.; Edwards, S. F. *The Theory of Polymer Dynamics*; Oxford University Press: New York, 1986.